December 10, 2012

Study of Muon Capture for Muon to Electron Conversion Experiments

AlCap Collaboration

D. Alexander[d], D.M. Asner[h], E. Barnes[b], R. Bernstein[c], R. Bonicalzi[h], A. Daniel[d], A. Edmonds[i], A. Empl[d], D. Hertzog[j], Y. Hino[g], E. Hungerford[d], T. Itahashi[g], D. Kawall[f], A. Kolakar[b], B. Krikler[e], P. Kammel[j], K. Kumar[f], Y. Kuno[g], A. Kurup[e], M. Lancaster[i], J. Miller[b], M. Murray[j], T.H. Nam[g], V. Ruso[c], H. Sakamoto[g], A. Sato[g], M. Schram[h], Y. Uchida[e], G. Warren[h], F. Wauters[j], P. Winter[a], M. Wing[i], L. Wood[h]

[a]Argonne National Laboratory, Illinois (ANL)
[b]Boston University, Boston, Massachusetts (BU)
[c]Fermilab National Accelerator Laboratory, Batavia, Illinois (FNAL)
[d]University of Houston, Houston, Texas (UH)
[e]Imperial College, London, UK (ICL)
[f]University of Massachusetts, Amhurst, Massachusetts (UMass)
[g]Osaka University, Osaka, Japan (OU)
[h]Pacific Northwest National Laboratory, Richland, Washington (PNNL)
[i]University College London, London, UK (UCL)
[j]University of Washington, Seattle, Washington (UW)

Co-spokespersons underlined.

Abstract

The recent observation that neutrinos oscillate, change flavour, and so have mass, requires an extension to the Standard Model (SM) and demonstrates that lepton flavour is not an absolutely conserved quantity. However, even when accommodating finite neutrino mass in a minimal extension to the SM, the rate of charged lepton flavour violating (CLFV) interactions is predicted to be far too small to be observed, $\mathcal{O}(10^{-50})$. Thus, any experimental observation of CLFV would be clear evidence of new physics beyond the SM.

Two new projects will search for the CLFV in $\mu^- N \to e^- N$ conversion. They are the Mu2e experiment at FNAL and the COMET experiment at J-PARC. Both experiments utilise multi-kW pulsed $8-9$ GeV proton beams to achieve a branching ratio sensitivity lower than 10^{-16}, that is 10,000 times better than the current best limit established by SINDRUM II.

Both COMET Phase-I and Mu2e are subject to significant backgrounds from the products from muon (and pion) nuclear capture. The goals of this joint proposal between both Mu2e and COMET collaborations are precision measurements of muon capture reactions in candidate targets, at levels required for the design and optimization of this new generation of experiments.

The initial focus of this proposal is on the measurement of low energy charged particles after muon capture on a nucleus. This process constitutes a severe background, and has inadequate experimental information available. X-rays and gamma-rays will be also observed, in order to verify that this technique can be used to determine the number of μ captures in a $\mu \to e$ experiment, and to normalize the proposed capture measurements. Finally we propose to study both neutron emission after μ capture and radiative decay of the μ in the nuclear environment as these also provide crucial information to be used in the design and simulation of the experiments.

PSI beam quality is critical to provide a pure, low-energy muon beam with a small momentum spread. This is especially important for charged-particle emission measurements, as thin targets of aluminum, silicon and titanium are required so that the emitted particles penetrate the targets with minimal energy loss. This was a major problem in previous experiments and has prevented the extraction of low-energy spectra.

Contents

1 Beam Requirements and Beam Request

Experimental area

πE1 beam line

Required beam properties

- Particle: μ^-
- Momentum: 30–35 MeV/c
- Momentum bin: < 2 % FWHM
- Beam spot: < 2 cm in diameter
- Intensity: 2×10^4 s^{-1}
- Beam purity: < 10 % electrons

Duration of the experiment

We request two 4 week PSI beam blocks, one scheduled in 2013 and the next one in 2014.

The first experiment would be used to commission the full set-up and shake down its components for the three work-packages (WPs) planned. The priority would be to perform most of the proton measurements (WP1), while simultaneously measuring the X-rays for WP2. A first exploratory neutron measurement to start WP3 is also anticipated. This part of the experiment is ready in spring 2013, and we would prefer an early running time during the 2013 schedule. After that, the data would be analyzed and results reported at the BVR 2014. Depending on the outcome, in 2014 additional proton statistics data taking and systematic studies are foreseen to achieve publication quality data. But the main focus in 2014 will be on final neutron measurements and operating the large NaI for the WP2 program.

The requested 2013 beam time will be structured in the following way:

- Week 1: Set-up. Commission beam counters, proton, X-ray and neutron detectors. Vacuum in target chamber.
- Week 2: Beam-optimization. Thick, then thin Si detectors as active targets are used to study beam properties and optimize the stopping fraction, to quantify background and select the optimal geometry of the detector packages, relative to target and beam. The X-ray detector will assist in the tuning process. First high statistics data set is taken with thin Si in the target position, to calibrate the target response function and normalize the X-ray detectors.
- Week 3: High statistics measurements with 3 targets of Al and Ti, 25-200 μm thickness.
- Week 4: Continued Al, Ti measurements. Last days dedicated neutron measurement, thick target, with proton vacuum chamber removed.

2 Safety

1. Radiation: standard PSI calibration sources will be used.
2. High voltages for photomultiplier and MWPCs: commercial and safety accredited HV supply units, cables and SHV connectors will be used.
3. Fire and explosion: no explosive material will be used in the experiment.
4. Cryogenic apparatus: liquid nitrogen may be used for the Ge detector, standard precautions will be taken.
5. The proton measurement uses an evacuated target chamber, with a mylar window of standard PSI beam window design.
6. Flammable gas with small flux (< 50 cc/min) will be used for the wire chamber; standard gas detectors and alarm system will monitor gas leaks.

3 Physics Motivation and Status

3.1 Introduction

A neutrino and a charged lepton form a natural doublet in the SM, and are assigned a flavor quantum number. The observation that neutrinos oscillate between flavours and thus have mass, means that lepton number is not absolutely conserved in the neutral lepton sector and this in turn means that lepton number is also not conserved in charged lepton interactions. However, due to the large difference in mass between the neutrino and the W boson, the branching ratio for charged lepton flavour violation (CLFV) in a minimal extension to the SM which includes massive neutrinos, is extremely small ($\mathcal{O}(10^{-50})$). Thus, any experimental observation of CLFV would be unambiguous evidence of new physics beyond the SM (BSM), and particle physics experiments searching for CLFV are amongst those with highest priority [1].

Most extensions to the SM predict rates for CLFV that are within reach of the next generation of experiments. Indeed current experiments such as MEG search for the CLFV process, $\mu^+ \to e^+\gamma$, and already place severe constraints on models of BSM physics. It is possible to construct a generic Lagrangian for BSM CLFV interactions [2] comprising dipole and contact interaction terms at a certain mass scale (Λ). The $\mu^+ \to e^+\gamma$ being probed by MEG, is mainly sensitive to dipole interactions whereas processes such as $\mu^+ \to e^+e^-e^+$ and the coherent neutrinoless transition of a muon in the field of a nucleus, $\mu^- N \to e^- N$, are mainly sensitive to contact interactions. Thus in order to elucidate the nature of any BSM physics it is necessary to make measurements of all three processes. In Fig. 1 the rates of CLFV are shown as a function of Λ and the relative contribution of the dipole and contact interactions (κ).

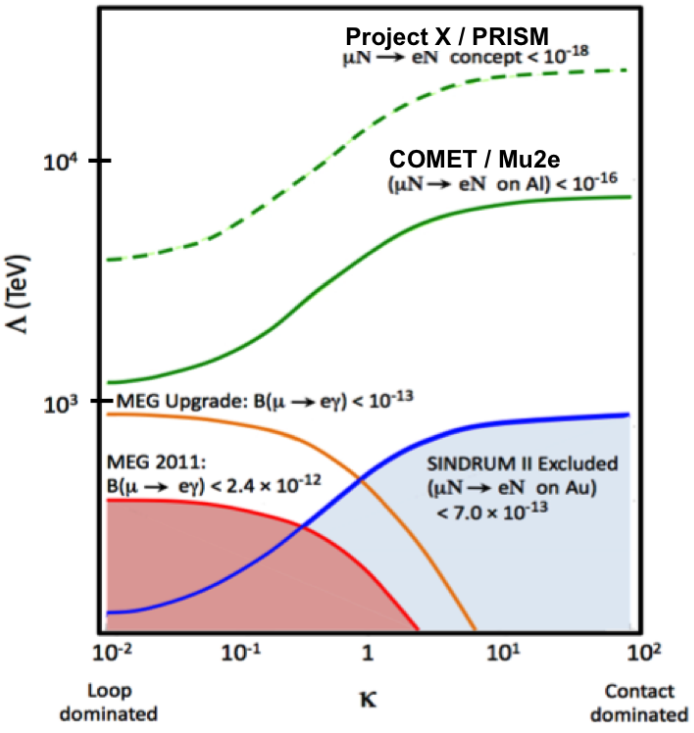

Figure 1: Branching ratios for two CLFV processes in a generic model of BSM physics having both dipole and contact interactions as a function of the scale (Λ) of the new physics.

It can be seen from Fig. 1 that CLFV processes potentially probe new physics at scales beyond the LHC. Dipole and contact interactions arise in many models of BSM physics. Supersymmetric interactions naturally provide dipole interactions which could result in significant rates for both the

$\mu^+ \to e^+\gamma$ and $\mu^- N \to e^- N$ processes while contact interaction terms arise in type-II Seesaw models that generate light neutrino masses through mixing with an additional massive neutrino. In general the Seesaw mechanism occurs at a very high mass scales ($\mathcal{O}(10^{10-14})$ GeV). CLFV effects are only large if additional new physics e.g. supersymmetry or extra dimensions are present at the TeV scale. In general CLFV processes probe physics both at the GUT-scale and the TeV-scale. Fig. 1 also highlights the necessity of searching for CLFV in both the $\mu^+ \to e^+\gamma$ and $\mu^- N \to e^- N$ process (and also the $\mu^+ \to e^+e^-e^+$ process) where the ratio of the branching ratios can yield information on κ.

The last search for $\mu^- N \to e^- N$ conversion was performed by the SINDRUM II collaboration at PSI. The SINDRUM II spectrometer consisted of a set of concentric cylindrical drift chambers inside a superconducting solenoid magnet of 1.2 Tesla. The experiment set an upper limit of $\mu^- N \to e^- N$ in Au of $B(\mu^- + Au \to e^- + Au) < 7 \times 10^{-13}$ [3]. Two new searches for CLFV in the $\mu^- N \to e^- N$ process are being pursued by experiments under construction in the USA (Mu2e [4]) and Japan (COMET [5]), both of which seek to probe the $\mu^- N \to e^- N$ process with a sensitivity better than $\sim 10^{-16}$. Schematic layouts of the experiments are shown in Fig. 2. For BSM interactions dominated by dipole operators these experiments have a similar sensitivity to the upgraded MEG experiment but have a far greater sensitivity to contact interactions.

The Mu2e and COMET experiments are seeking to improve on the SINDRUM II sensitivity by a factor of 10,000. Both experiments utilise multi-kW pulsed proton beams of energy 8–9 GeV produced by the FNAL (Mu2e) and J-PARC (COMET) accelerator complexes. Mu2e received CD1 DOE approval in July 2012 and the staged construction of COMET was approved in March 2012 and construction of the beamline will begin in 2013. In the Phase-I COMET experiment, shown in Fig. 3, there is a reduced beamline and a cylindrical drift chamber will immediately surround the target where the muons are captured. Thus, it is very sensitive to the products of muon (and pion) nuclear capture. In Mu2e there is a similar sensitivity since the straw tracking detector is immediately downstream of the muon target.

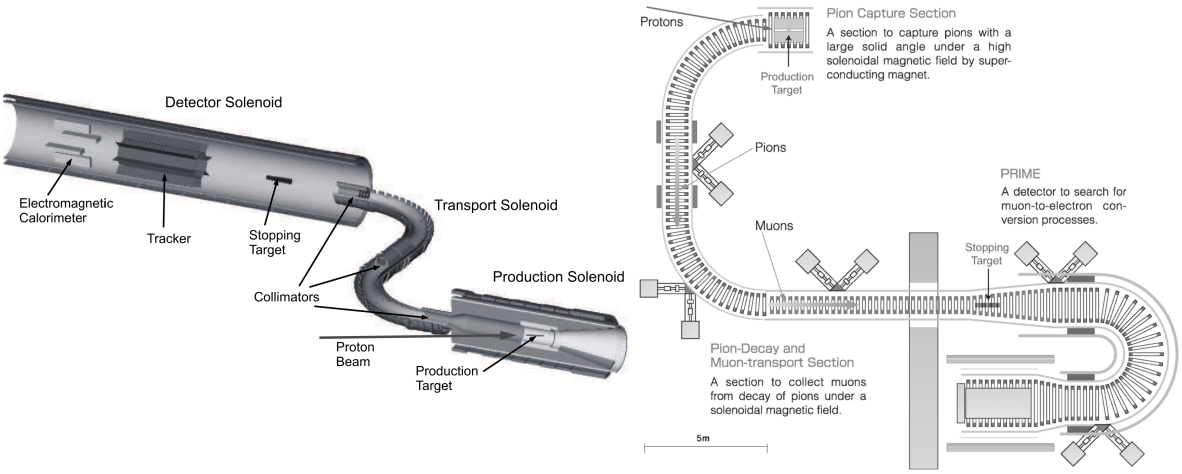

Figure 2: Schematic layouts of the Mu2e (left) and the COMET Phase-II experiments (right).

The $\mu^- N \to e^- N$ process is particularly attractive since the experimental signature is very straightforward: a single mono-energetic electron with an energy of approximately $m_\mu - B$ where B is the binding energy of the muon in the $1s$ level in the muonic atom (N). This single particle signature does not suffer from the accidental background which occurs when coincidences are required; e.g. between e^+ and γ in the $\mu^+ \to e^+\gamma$ process. This is a particularly important, limiting background at high muon rates. The energy of the mono-energetic electron from the $\mu^- N \to e^- N$ process has far higher energy than in Michel decays, and for μ decays in orbit (DIO) the phase space for electron energies approaching the endpoint rapidly vanishes.

In addition to the DIO process or the CLFV process a muon in the $1s$ state in a muonic atom can be captured by the nucleus via the process: $\mu^- + N(A,Z) \to \nu_\mu + N(A, Z-1)$. In general this process is

also accompanied by the emission of photons, neutrons and charged particles (particularly protons) and it is the measurement of these emitted particles that is the subject of this proposal. In order to optimize $\mu \to e$ experiments, it is important to accurately know the rate and energy spectra of these particles, since they can form significant backgrounds, degrade the efficiency of electron tracking, and damage the readout electronics. Photons can Compton scatter or convert, producing electrons which cause ambiguities in track reconstruction and degrade detector resolutions. In addition to these problems, low energy protons can saturate the electronic amplifiers due to large energy losses, and prematurely "age" detector components. Neutrons cause recoil protons and can get captured, producing photons. Low-energy neutron cross sections are large and are difficult to shield. They can cause significant radiation damage. Monte-Carlo simulations of these nuclear capture processes rely on spectra data taken over twenty years ago for a limited number of nuclei in a restricted energy range. Low energy energy neutron spectra are particularly dependent on the nucleus. The motivation for this proposal is to make precision measurements for the target materials that will be used by Mu2e and COMET over the entire relevant energy region.

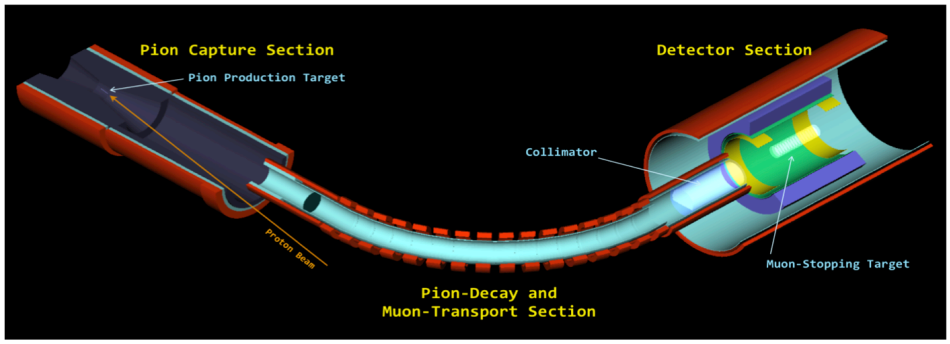

Figure 3: The COMET Phase-I detector where a cylindrical drift chamber immediately surrounds the muon stopping target and is therefore subject to the products of the nuclear muon capture process.

3.2 Experimental Goals and Physics Processes

As outlined in the introduction, the Mu2e and COMET collaborations propose to study background reactions to the $\mu^- N \to e^- N$ process for the candidate target materials (Al, Ti). These studies are needed to optimise the designs of the two experiments, as existing information on these background processes is limited and what is known, is insufficiently precise. The new piE1 beamline at PSI offers a unique opportunity for these experiments, as emphasized in section 3.3. Our experimental program is organised in three distinct work packages (WP), directed by different team leaders, given in parentheses.

WP1: (Kammel (Seattle), Kuno(Osaka)) **Charged Particle Emission after Muon Capture.**
Protons emitted after nuclear muon capture in the stopping target dominate the single-hit rates in the tracking chambers for both the Mu2e and COMET Phase-I experiments. We plan to measure both the total rate and the energy spectrum to a precision of 5% down to proton energies of 2.5 MeV.

WP2: (Lynn(PNNL), Miller(BU)) **Gamma and X-ray Emission after Muon Capture.**
A Ge detector will be used to measure X-rays from the muonic atomic cascade, in order to provide the muon-capture normalization for WP1, and is essential for very thin stopping targets. It is also the primary method proposed for calibrating the number of muon stops in the Mu2e and COMET experiments. Two additional calibration techniques will also be explored; (1) detection of delayed gamma rays from nuclei activated during nuclear muon capture, and (2) measurement of the rate of photons produced in radiative muon decay. The first of these would use a Ge detector and the second a NaI detector.

The NaI calorimeter will measure the rate of high energy photons from radiative muon capture (RMC), electrons from muon decays in orbit (DIO), and photons from radiative muon decay (RMD), as potential background sources for the conversion measurement. As these rates are expected to be extremely low near the conversion electron energy, only data at energies well below 100 MeV will be obtained.

WP3: (Hungerford(UH), Winter(ANL)) **Neutron Emission after Muon Capture.**
Neutron rates and spectra after capture in Al and Ti are not well known. In particular, the low energy region below 10 MeV is important for determining backgrounds in the Mu2e/COMET detectors and veto counters as well as evaluating the radiation damage to electronic components. Carefully calibrated liquid scintillation detectors, employing neutron-gamma discrimination and spectrum unfolding techniques, will measure these spectra. The measurement will attempt to obtain spectra as low or lower than 1 MeV up to 10 MeV.

WP1 is the most developed project in this program. Most of the associated apparatus has been built and optimized. We are ready to start this experiment in 2013, while preparing and completing test measurements and simulations to undertake WP2 and WP3.

3.2.1 WP1: Charged Particle Emission after Muon Capture

Present knowledge

The yield, energy spectrum and composition of the charged particles emitted in muon capture on Al and Ti have not been measured directly in the relevant energy range for COMET Phase-I and Mu2e. Only high energy spectra are available for Al (Fig. 4), while low energy spectra are only measured for Si (Figure 5), where muons can be stopped and captured in an active silicon detector [6]. The peak below 1.4 MeV is presumed to be due to recoiling heavy ions, mainly ^{27}Al, when no charged particles were emitted. Hungerford [7] fitted the silicon spectrum in Fig. 5 with an empirical function given by;

$$p(T) = A(1 - \frac{T_{th}}{T})^{\alpha} e^{-(T/T_0)} \quad (1)$$

where T is the kinetic energy and the fitted parameters are $A = 0.105$ MeV^{-1}, $T_{th} = 1.4$ MeV, α=1.328 and $T_0 = 3.1$ MeV. The spectrum is normalized to 0.1 per muon capture. Some other results in the past experiments are summarized in Table 1.

Relevance for $\mu - e$ Conversion Experiments

The tracking detectors of COMET Phase-I and Mu2e are designed to measure the helical trajectories of 105 MeV conversion electrons in a uniform, cylindrical magnetic field. The detector geometry coupled with the field strength accepts charge particle momenta between 54 to 200 MeV/c. In this momentum range "hits" in a tracker plane are dominated by proton emission after nuclear muon

Table 1: Probabilities in units of 10^{-3} per muon capture for inclusive proton emission from [8]. The numbers in crescent parenthesis are estimates for the total inclusive rate derived from the measured exclusive channels by the use of the approximate regularity, such as $(\mu, \nu p) : (\mu, \nu pn) : (\mu, \nu p2n) : (\mu.\nu p3n) = 1 : 6 : 4 : 4$.

Target nucleus	Calculation	Experiment	Estimate	Comments
$^{10}_{}$Ne		200 ± 40		
$^{27}_{13}$Al	40	$> 28 \pm 4$	(70)	7.5 for $T > 40$ MeV
$^{28}_{14}$Si	144	150 ± 30		3.1 and 0.34 d for $T > 18$ MeV
$^{31}_{15}$P	35	$> 61 \pm 6$	(91)	
$^{46}_{22}$Ti				
$^{51}_{23}$V	25	$> 20 \pm 1.8$	(32)	

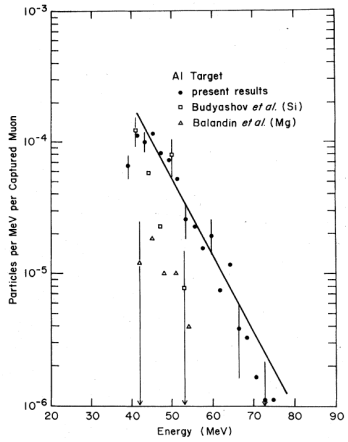

Figure 4: Energetic charged particle spectrum from muon capture in Al and other targets [9].

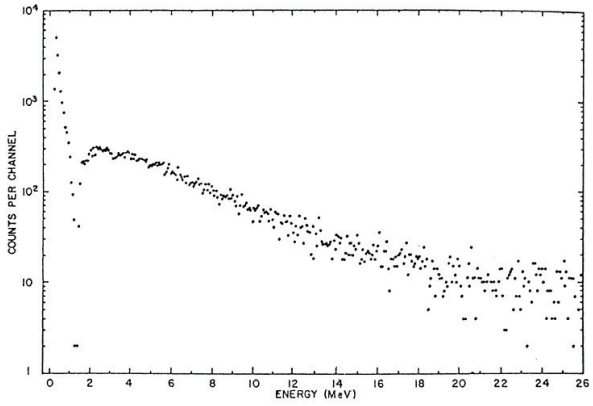

Figure 5: Charged particle spectrum from muons stopping and being captured in a silicon detector [6].

capture. Such events are particularly troublesome due to their large energy deposition. In addition to protons, electrons emitted during muon decays in orbit (DIO) are also a source of background. Background events in the tracking detector can produce ambiguous track reconstructions, which may lead to mis-identified events in the signal region. Both experiments plan to introduce thin, low-Z proton absorbers in front of the tracking chambers to reduce proton hit rates. These are effective at removing protons due to their very low energies (5 MeV for 100 MeV/c protons). However, such absorbers degrade the momentum resolution of conversion electron candidates and their thickness and geometry must be carefully designed. For similar reasons, the design of the stopping target is also important. The limited information available at present makes it difficult to arrive at a conclusive detector design. From Table 1, the relative experimental yield for proton emission from Al for energies above 40 MeV is 3%. From theory the expectation is 4%, if estimated from the ratio of exclusive channels from other nuclei it is 7%, or it may be as high as that from Si or Ne, 15-20%. The energy spectrum can only be inferred from the Si data or from Ref. [10]. At this moment, [10] has been used to estimate proton emission for both experiments. The emission of deuterium and alpha particles is also not known. Charged particle yields from Ti can only be estimated from V to be around 3%. Thus a measurement of the rate and spectrum of proton emission after muon capture is required in order to estimate background and optimize the detector design.

In COMET Phase-I, singles rates in the tracking chamber (cylindrical drift chamber) have been estimated based on the spectrum given in Eq.(1). To reduce the proton flux entering the tracking chamber, in addition to the inner wall of the drift chamber (of 400 μm) a cylindrical proton absorber is located in front of the tracking chamber. Monte Carlo simulations were run for three different thicknesses of proton degrader, 0 mm, 5 mm, and 7.5 mm and are are summarized in Table 2, where the proton emission rate of 0.15 per muon capture is assumed. For a typical number of stopped muons and for a 5 mm degrader, the total number of hits in the first plane is estimated to be 530 kHz (1.3 MHz). According to simulations, rates are similar for Mu2e. In simulation studies of reconstructed conversion electron tracks mixed with a nominal proton background, a decease of approximately 17% in energy resolution in the conversion electron peak and a down shift of 0.7 MeV was found when a standard proton absorber was inserted. A downshifted conversion peak is an issue as it pushes the signal up the DIO background curve.

Table 2: Total numbers of hits in the first layer by protons emitted from muon capture for different trigger counter thickness. 100 k proton events were generated for COMET Phase-I. 15 % protons per muon capture is assumed.

proton degrader thickness	0 mm	5 mm	7.5 mm
hits	2644	103	30
hits per proton emission	2.6 %	0.1 %	0.03 %
hits per muon capture*	3.9×10^{-3}	1.5×10^{-4}	4.5×10^{-5}

3.2.2 WP2: Gamma and X-ray Emission after Muon Capture.

Present knowledge

When a negative muon is captured in an atomic orbit, it cascades down to the 1s level within 10^{-13}s. Initially the cascade occurs with Auger emission, but near the $n = 5$ atomic level, muonic X-rays start to dominate the process. Theoretical determination of the energy levels is complex, due to effects such as screening of the nucleus by inner electrons, shift of low-level states due to the finite charge distribution of the nucleus, relativistic corrections, and fine structure splitting of levels. Nevertheless, muonic X-rays have been used to identify the capturing element, typically from the $2p \rightarrow 1s$ transition X-ray, which occurs ∼80% of the time. An X-ray spectrum for phosphorus is shown in figure 6.

The spectra of prompt gammas from muon capture have been measured for Al [11] but not for Ti, using time coincidences with the incoming muon. To our knowledge there are no data for singles mode or for delayed gammas from decays of unstable nuclei produced in the muon capture process.

The RMD photon spectra have been measured in previous experiments (including MEG) and is theoretically well reproduced for a free muon. We propose to evaluate the feasibility of measuring the spectrum using a NaI detector for energies between 20 and 54 MeV. In this region the spectrum is only slightly distorted by the fact that the muon is bound in an atomic orbit.

We also propose to confirm with existing data, the high energy tail of the electron and photons from RMD, DIO, and RMC. We note that the high energy tails for RMD and DIO are the result of atomic binding, which is absent in free muon decay. There is a recent theoretical calculation [12] of the DIO electrons which should be tested. Due to rates at PSI, we would only be able to observe spectra at energies below 80 MeV. The spectra near the end-point energy can only be observed with the extremely large number of stopped muons envisioned in the Mu2e and COMET experiments.

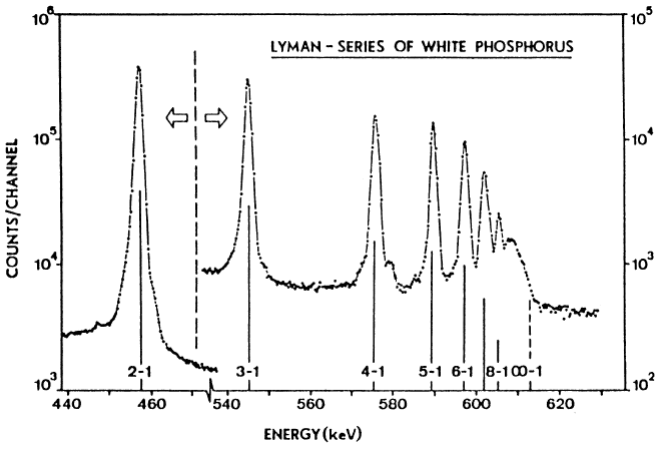

Figure 6: A typical muonic X-ray spectrum [13].

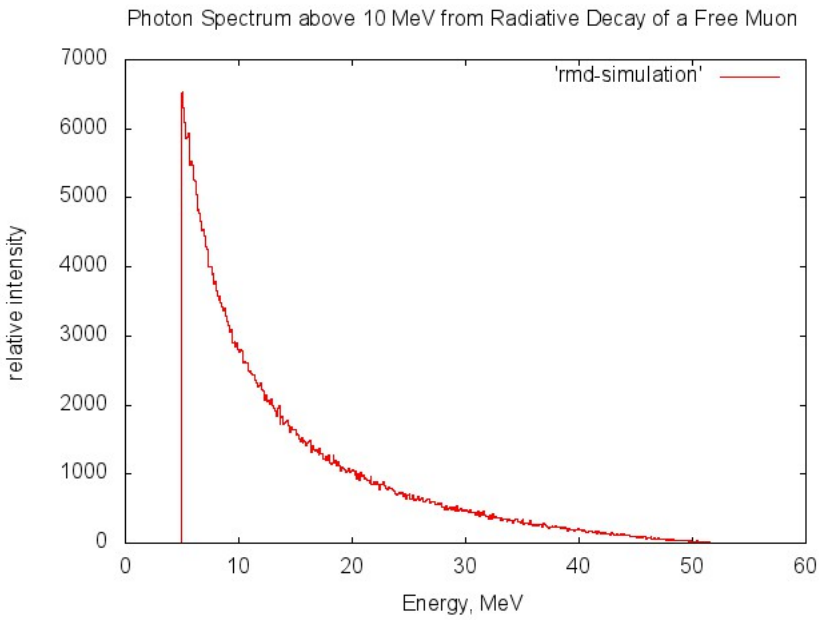

Figure 7: A typical radiative muon decay spectrum.

Relevance for $\mu - e$ Conversion Experiments

The rate of muon capture in the stopping target is critical for proper normalization of data in the $\mu^- N \to e^- N$ experiments, and the proposed method of observing this rate will count muonic X-rays as the $\mu \to e$ data are collected. A germanium detector will be placed far from the stopping target to reduce both rate and damage to the detector. A dipole magnetic field will be used to remove charged particles moving along the field of view from the detector to the target. However, the environment will be challenging, as high photon rates and a significant neutron background will be present. Pacific Northwest National Laboratory is currently developing high-rate germanium detectors utilizing such methods as custom fast preamplifiers and segmented detectors. Measurements using these designs in muon beam tests at PSI will be invaluable proofs of principle for the Mu2e experiment. Also, identifying how the gamma and neutron backgrounds affect the gamma and X-ray lines as a function of dose is of critical importance.

In the past, experiments that have studied muonic X-ray spectra used time coincidence between the observed X-ray and the incident beam muon. In the Mu2e experiment, the muon beam will be pulsed, with an average muon stopping rate in excess of 10^{10} Hz. This is too large for a beam gate to tag muon arrival. Thus, it is necessary to operate the Ge detector in singles mode, and the PSI measurements are essential to determine whether the X-rays can be detected above background in this situation.

In case background in singles mode are too severe, two alternate means to monitor the Mu2e stopping rate will be evaluated. In one of the alternatives, simultaneously with the collection of muonic X-ray spectra, we will search for delayed gammas arising from the decay of nuclei activated by nuclear muon capture. For example, in the case of muon capture on ^{27}Al, the reaction $^{27}\mathrm{Al}(\mu^-, \nu)^{27}\mathrm{Mg}$ occurs in 16% of the captures. The lifetime of the ^{27}Mg is 9.458 minutes. It decays to excited states in ^{27}Al, leading to a 1014.45 keV gamma 21% of the time, and an 843.76 MeV gamma 100% of the time. In normal operation, Mu2e will have a steady stream of 8 GeV proton pulses on the production target (spaced at 1.5 microsecond intervals) for about 0.4 s, followed by about 0.9 s period of beam-off. It may be possible to observe the ^{27}Mg decays with a Ge detector in the reduced background environment when the beam is off. At PSI, we would test whether these gammas can be cleanly separated from background. Another normalization alternative would be the measurement of energetic photons from the radiative decays of the muons bound in atomic orbits in the stopping target (RMD). Similar to free muon decay, the branching ratio for photons above 10 MeV relative to regular decay is about 1.4% and the energy distribution peaks at low energy, uniformly decreasing up to about 54 MeV (see

Fig. 7). Above 54 MeV, the free muon probability is zero, but the energy endpoint actually goes above 100 MeV for bound μ^-, albeit with very small probability. In addition to this inner bremsstrahlung process, there will be a calculable contribution from the bremsstrahlung of electrons from the dominant decay mode of the muon, DIO. At energies above 10 MeV, the backgrounds are much less than at lower energies, possibly allowing a good signal to background ratio for a normalization measurement. Using tagged electrons from DIO, we would measure RMD as well as DIO rates. Photons from RMD (and hence electrons from pair production in the target surrounding materials) and electrons from DIO have endpoint energies equal to the conversion electron energy, with probabilities decreasing rapidly as the energy approaches the endpoint. These potential backgrounds are controlled with sufficiently good conversion electron energy resolution. We note that using RMD photons may not be as clean as using muonic X-rays or activation gammas, depending on the quality of photon collimation to the detector, since the RMD spectrum is not unique to the target species, and the energy distribution is not ideal, dropping rapidly with increasing energy.

A NaI calorimeter will be used to measure the higher energy photons and electrons from RMD and DIO. We have access to a large NaI detector, however we are searching for a more easily managed small array of crystals for this task which will be easier to transport, mount, and shield. With the implementation of an NaI calorimeter, we have the additional possibility to affirm old measurements of the rate of radiative muon capture (RMC) at energies from 55 MeV (just above the bulk of the muon decay flux) to about 75-85 MeV (where the rate becomes too small to measure at the integrated fluxes envisioned at PSI). The branching ratio is on the order of 10^{-5}. Pair production from the photons produce electrons detectable above background in approximately the same energy range, with the precise endpoint depending on the rest energies of the daughter nuclei

3.2.3 WP3: Neutron Emission after Muon Capture

Present knowledge

Nucleon emission after muon capture, particularly the nuclear dynamics, is not well understood. Neutron emission is described by direct and evaporative processes with energies ranging from thermal up to some 50 MeV. However, most neutrons, at least for heavy nuclei, are emitted by evaporation after an excited nucleus is formed. Theoretical studies indicate that giant resonance levels, [8, 14] are important doorways leading to neutron emission. If this is the case, the reaction occurs through a two-step process as described by;

$$\begin{aligned} \mu^- + A(N,p) &\rightarrow \nu_\mu + A(N+1,p-1)^* \\ A(N+1,p-1)^* &\rightarrow xN + x'p + x''\gamma \end{aligned} \tag{2}$$

In the above reactions, the x's represent emission of any number of particles including photons as the nucleus de-excites. If neutrons are emitted from giant resonance excitation, broad peaks at lower energies would be expected and are observed, Figure 8 [15]. Also, one would expect multi-particle emission, as has indeed been observed for various targets [16, 17]. Multiplicity measurements for targets of relevance (close to Atomic Numbers of Al and Ti) are shown in Table 3.

Table 3: Neutron multiplicities for various targets. The distribution is adjusted to 0.545 [16].

		Multiplicity			
Target	Avg. Mult.	0	1	2	3
Al	1.262 ± 0.059	0.449 ± 0.027	0.464 ± 0.028	0.052 ± 0.0013	0.036 ± 0.007
Si	0.864 ± 0.072	0.611 ± 0.042	0.338 ± 0.042	0.045 ± 0.0018	0.000 ± 0.008
Ca	0.746 ± 0.032	0.633 ± 0.021	0.335 ± 0.022	0.025 ± 0.0009	0.004 ± 0.006
Fe	1.125 ± 0.041	0.495 ± 0.018	0.416 ± 0.019	0.074 ± 0.0011	0.014 ± 0.005

At higher energies, direct emission involves photo-production on a proton in the nucleus, with the emission of a neutron. The end-point energy of this process is approximately 6 MeV for at rest

protons, but protons move with Fermi motion in the nucleus so an energy spectrum is produced. Thus correlated proton-neutron emission and proton-photon emission would be expected. Examples of this are described in radio-chemical experiments [17].

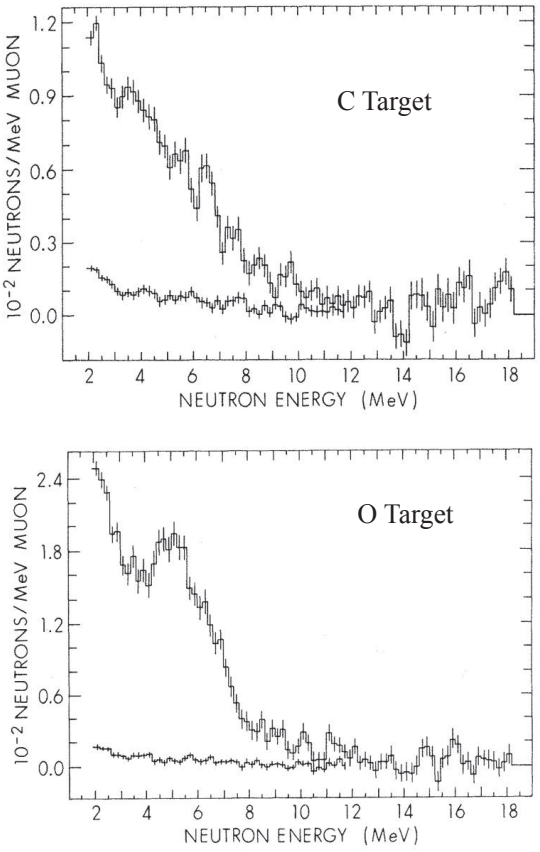

Figure 8: Spectra of neutron energies after muon capture showing emission from giant resonance excitations in C (above) and O (below). Note the rise in evaporative emission at low energies [15].

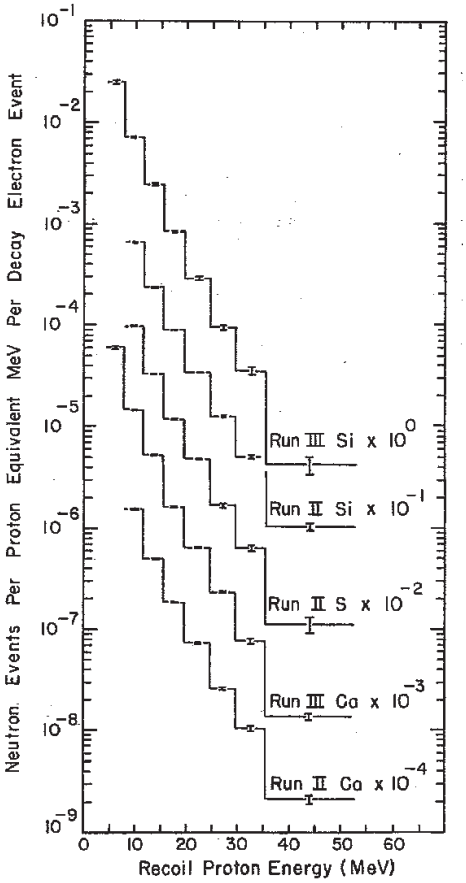

Figure 9: Higher energy neutron spectrum for various light nuclei. Note the exponential decrease with energy [18].

A number of experiments studied high energy neutron emission from targets as light as Si in order to observe the neutron asymmetry. In the process of such measurements neutron spectra were extracted [18] and examples are shown in Figure 9. These spectra have a low energy cut-off ranging from 4 to 10 MeV as only direct emission is expected to preserve asymmetric emission. They are consistent with an exponential decrease as a function of increasing energy, and show no indication of an evaporative increase or resonance emission at lower energies. However, the break in the slope of the spectrum in heavier nuclei occurs around 10 MeV, and evidence of a spectrum break may have been missed due to the energy cut off . From these data on Si, the measured number of emitted neutrons per muon capture above approximately 4 MeV is approximately 0.43. This experimental result is corrected for multiple neutron emission which is small, at least at the measured energies.

In summary, the neutron energy spectrum seems reasonably determined for neutron energies above 10 MeV. Low energy emission depends on nuclear structure and is less well defined. At energies of less than a few MeV there is an evaporative increase as well as emission from giant resonant states.

Relevance for $\mu - e$ Conversion Experiments

The Mu2e and COMET experiments stop negative muons in an ^{27}Al target. The signal of interest is an electron, emitted with approximately 100 MeV/c momentum. The Mu2e tracking detector, which is constructed of straw-tubes or a drift chamber, is relatively insensitive to neutrons, but this is not the case for the calorimeter, the cosmic ray veto scintillators, and the readout electronics inside the detector solenoid. There is a large flux of neutrons from the production target which is reduced by shielding between the production and detection solenoids. With this shielding in place, simulation shows that neutrons from muon captures in the stopping target then dominate the neutron background in the tracker, Table 4. Due to their proximities, neutron backgrounds in the cosmic ray veto, and particularly the calorimeter, are more sensitive to neutrons emitted after muon capture in the beam-stop.

Table 4: Neutron Background Sources on the Tracker as a function of Neutron Kinetic Energy, T

	Neutrons/cm^2 ($\times 10^{10}$)		
Source	Thermal($T < 1$ eV)	Epithermal (1eV $< T <$ 1 MeV)	Fast ($T >$ 1 eV)
Stopping Target	16	77	100
Muon Beam Stop	0.2	2	0.8
Beam Flash	0.2	1	2
Production Solenoid	0.6	0.09	0

Aside from radiation damage to the electronics, fast neutrons cause single event upsets (SEU) during dynamic operations in electronic systems. Depending on the upset, redundancy, and software verification, these either could be ignored, result in data contamination, or in electronic failure. A dose of $5 \times 10^4\, n/s/cm^2$ was found using a MARS estimate of the neutron spectrum from the stopping target (see Fig. 10). Thus, for a nominal IC area of 1cm2, each IC must be tolerant to about 10^{12} neutrons which would be expected in 4×10^7 beam-on-target seconds. Better limits on these estimations should be obtained.

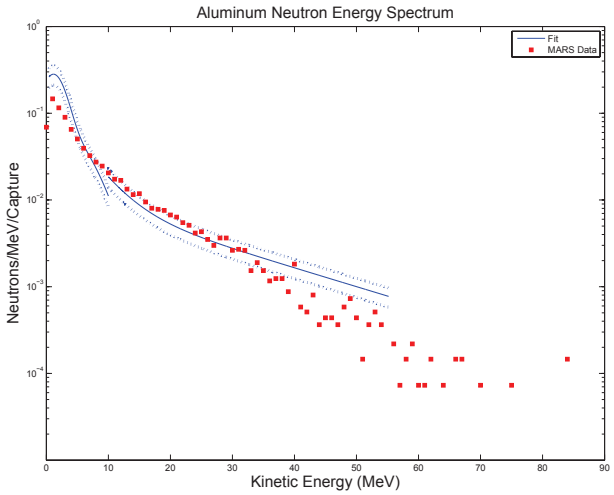

Figure 10: The neutron energy spectrum after emission from an Al Target as obtained from a MARS Simulation and used as input to neutron background calculations

Many muons, protons, and photons produced in the stopping target reach the calorimeter. The estimated rates of neutrons and gammas in the calorimeter are approximately 300 kHz and 85 kHz, respectively. Simulation shows this introduces pileup probabilities of 40% and 20%, but with average energy depositions of 0.5 MeV and 0.7 MeV, respectively.

Background (e.g. false cosmic ray vetoes) in the cosmic ray veto, CRV, must not affect live time by more than 1%. Most neutrons reaching the CRV have kinetic energies below 10 MeV, with the most probable energy about 1 MeV. The CRV is shielded by concrete and most likely Boron loaded polyethylene, the thickness to be determined by shielding simulations. The CRV scintillator (C8H8) is sensitive to neutrons which capture and scatter on protons with a cross section increasing with decreasing energy (1/velocity for the captures). Thus thermal and epithermal neutron energies are most important. These neutrons would be produced by attenuation of MeV neutrons as they penetrate the shielding between the CRV and the stopping target or the beam dump. Simulation studies for the neutron spectrum at the CRV use Geant3 GCALOR with an input spectrum from MARS as shown in Fig. 10. This spectrum is certainly not correct at low energies as seen when compared to the C and O experimental data in Figure 8 above. Thus since detector design and simulation are based on input of estimated neutron emission, as discussed above, it is important to obtain reliable experimental measurements for calibration. As examples, we must know the impact of radiation effects on the electronics, and must design the detectors to reduce the effects of neutron backgrounds.

3.3 Project History and Unique PSI Capablities

An initial test run for measuring protons emitted from Al targets was performed by a subset of this collaboration at PSI in 2009. It helped to commission part of the apparatus used for the current proposal. It also showed deficiencies which helped to define and optimize the set-up proposed here. In particular, the beam quality, the X-ray detection, the thin dE/dx detectors, the shielding of stray muons etc. need additional careful attention.

In 2012, a joint COMET/Mu2e project on charged particle emission was started, when the high relevance of proton emission for the new COMET Phase-I idea was realized. Due to the geographical advantage of Vancouver, as a good crossing point for the Fermilab and J-PARC collaboration, a proposal [19] was submitted to TRIUMF in summer 2012, and accepted with high priority. The PAC recommendation reads:
"The proposed set of muon capture background measurements are deemed crucial to the design and understanding of future neutrino-less muon-to-electron decay experiments, such as COMET and mu2e. Thus the committee approves this proposal with high scientific priority. It is noted that it is not yet clear which muon beamline will be available for this study with the desired negative muon properties. Once a suitable beamline has been identified that will be ready and available on the required timescales, the committee recommends that the full 36 shifts be granted."

Unfortunately, the above-mentioned availability of a suitable beamline for low energy μ^- turned out to be a problem. The allocated test beam times in fall of 2012 could not be realized, as the M9B beamline experienced vacuum problems at the T2 target station as well as difficulties with the superconducting decay channel. Moreover, TRIUMF cloud beamlines with better momentum bin essential for this experiment, are not foreseen to be operated with negative muons. In this situation, the collaboration asked the TRIUMF management to put S1371 on standby.

Meanwhile, PSI built a new low energy muon beam for particle physics, initially for the MuSun experiment. This beamline was successfully commissioned by the MuSun collaboration, including some members of the present collaboration. The results were extremely positive. In particular, the beamline appears to be the world-wide superior channel for experiments needing muon beam *at low energies with very narrow energy spread*. This advantage is due to the high proton intensity at PSI, combined with a special cloud muon channel, which selects the momentum with three bending magnets and thus allows for a dispersive focus. The initial commissioning results by the MuSun collaboration promise excellent conditions for the thin targets anticipated in AlCap. Further beam details are discussed in the MuSun progress report, submitted to this BVR.

4 Experimental Strategy and Equipment

4.1 Charged Particle Emission after Muon Capture

The goal of the experiment is a measurement of the rates and energy spectra of charged particle emission after muon capture in; 1) the favored conversion target, Al, 2) in Si (as normalization and cross check), and 3) Ti (as an alternative conversion target material). Both the rate and energy spectrum would be measured at 5% precision down to an energy of 2.5 MeV.

The basic requirements are summarized is Fig. 11. As the emitted charged particles deposit a significant amount of energy during their passage through the target material, thin targets and thus excellent momentum resolution of the low energy muon beam are critical for the experiment. This is exactly the reason, why the older experiments, which were performed with thick targets and less sophisticated beams, are unsuitable for providing the required yield and spectral information at low energies. The observed energy spectrum $g(T_f)$ of protons emitted from the stopping target is a convolution of the initial capture spectrum $f(T_i)$ with a response function $k(T_f, T_i)$:

$$g(T_f) = \int_0^\infty k(T_f, T_i) f(T_i) dT_i \tag{3}$$

The response function can be readily calculated for a uniform muon stopping distribution within the target depth. The resulting distortion of the original energy distribution taken from Equ. 1 is illustrated in Fig. 12 for different target thickness.

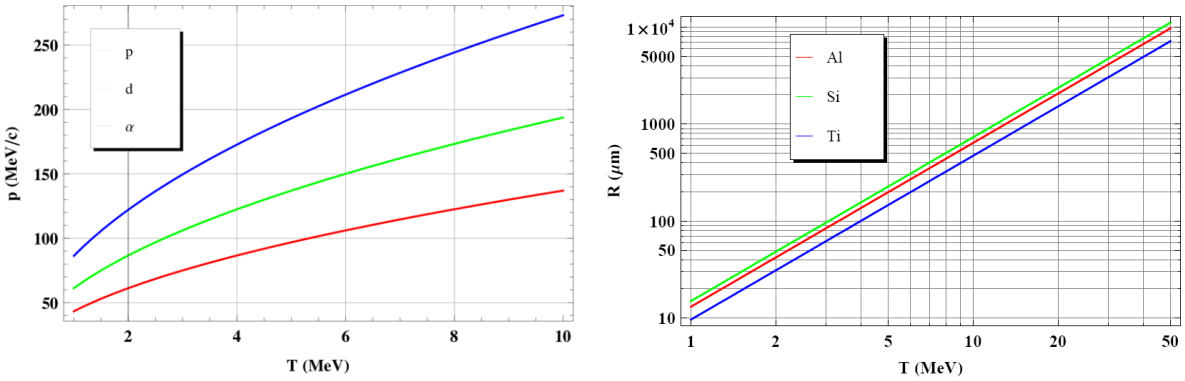

Figure 11: Left: Momentum vs. energy for p, d, α, right: proton range vs. energy in targets.

A schematic layout of the experimental setup is shown in Fig. 13. It will be an improved version of a test experiment performed by part of this collaboration at PSI in 2009.

Low energy muons will be detected by external beam counters (scintillator and wire chamber, not shown). The muons then enter a vacuum vessel though a thin mylar window and a fraction stopped in passive Al and Ti foils of 25 to 100 μm thickness. These foils are aligned 45 degrees with respect to the beam direction. As a cross check, muons will also be stopped in active Si detectors used as targets. Two packages of charged particle detectors are positioned on opposite sides, perpendicular to the target surface. The geometry is chosen so as to minimize the path length of the emitted protons, and limit their direction to be nearly perpendicular to the detectors. This improves the PID resolution by dE/dx separation. The main detector of the package is a 5×5 cm^2 Si detector of 1500 μm thickness (MSX), which will stop protons up to about 12 MeV. Plastic scintillators positioned behind this Si detector observe higher energy protons and veto through-going electrons. To provide dE/dx information some data will be taken with two 10x10 cm^2 thin Si detectors (65 μm, MSQ). These detectors are 4-fold segmented. Since their large capacitance deteriorates the overall resolution, measurements with and without them are foreseen. The symmetry between the left and right Si stations allows for a powerful monitor of systematic effects. Differences between the detectors would indicate background due to different stopping materials, non–uniform stopping distributions, or differences due to muon scattering. Careful shielding of direct or scattered muons is required, as the stopping fraction is small

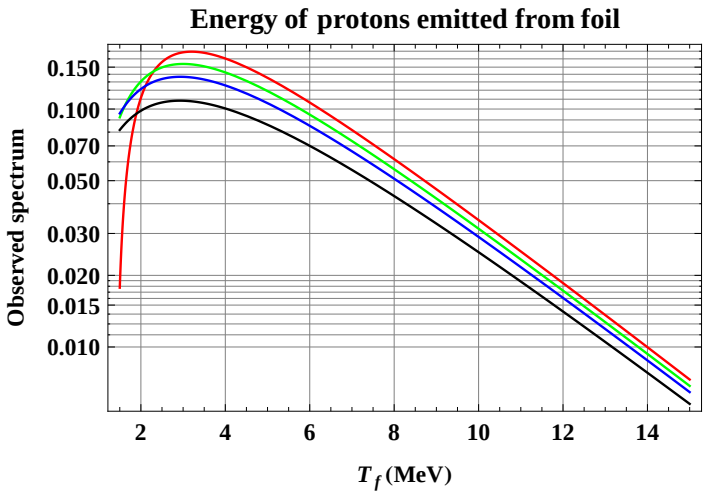

Figure 12: Calculated proton emission spectrum as function of target thickness (red: 0 μm, green: 50 μm, blue: 100 μm, black : 1000 μm).

and proton emission is a rare capture branch. As shown, we are considering a geometry, where there is no direct line of sight between any low Z material exposed to muons. Thus, all shielding uses lead.

In order to normalize the number of muon-stops in the aluminum target, a Germanium detector will be used to measure muonic X-rays from muons that stop in the aluminum target. We also will have telescopes to detect electrons from muons for an additional normalization of muon-stops.

The main systematic issues are as follows.

- Deconvolute the original proton spectrum $f(T_i)$. An optimal cloud muon beam is requested for the experiment. Then an active Si target allows an experimental calibration of the response function, because both T_i and T_f are accessible with an active target.
- Absolute calibration. The number of muon stops will be determined with the Ge detector. Again, the use of an active Si target allows a cross calibration. The proton detection efficiency will be simulated by Geant and calibrated with the active Si target.
- PID. The PID of emitted charged particles will be determined by dE/dx. The use of time of flight will be investigated.
- Background. Electron background will be determined with μ^+, neutron recoils by absorbing the proton component before the Si detectors. A dangerous background are muons stops in walls and scattered into the Si detector.[1]

A realistic Geant4 simulation is being developed. It will serve as an important tool to optimize the geometry, in particular the investigation of the background and response function. Currently the geometry of the PSI test run is being implemented for a realistic check of the simulation.

Figure 14 shows Monte Carlo simulation studies of two-dimensional plots of energy in the MSQ counter (dE/dX) vs. energy of the MSX counter. From Fig. 14, it is clearly seen that we can discriminate protons, deuterons, scattered muons, and electrons up to 10 MeV.

The event rates are estimated based on Monte Carlo simulation. Preliminary results are summarized in Table 5. They will be updated once we have full information about the PSI beam properties. As seen in Table 5, proton rates are not large. Additional collimation, if required to obtain background reduction, and the low muon momenta, which might require the use of degraders, may further reduce the rates below these estimates. A muon beam of low and well defined momentum is of critical importance.

[1] If the low energy target scattering is too high, we are also studying a configuration, with the two Si detectors positioned symmetrically and perpendicular to the beam.

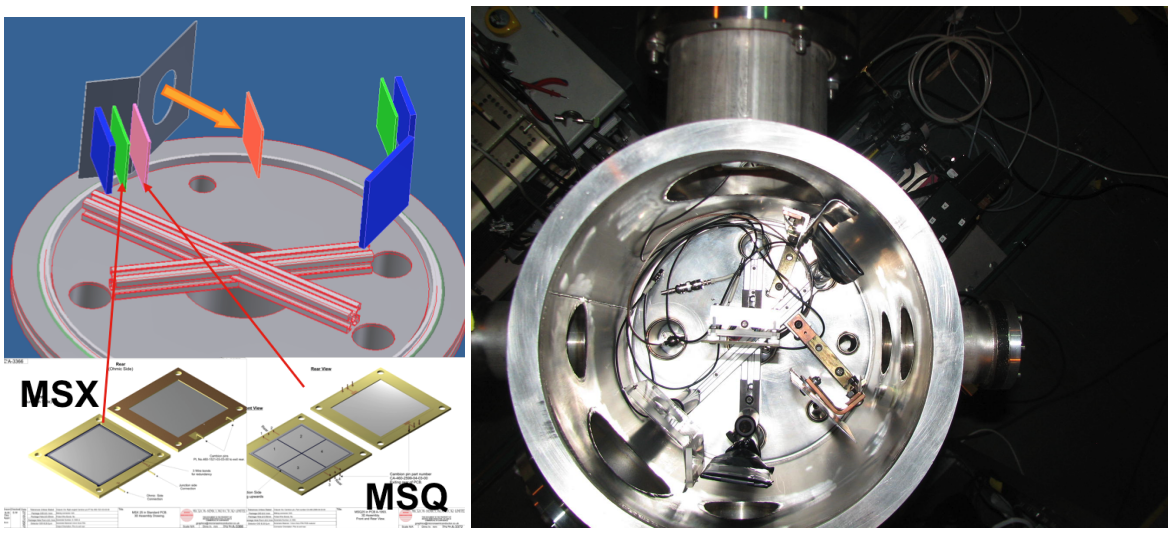

Figure 13: Left: CAD of layout, right: picture of vacuum vessel with detectors.

Table 5: Estimated event rates for various targets of different thickness. Incoming 10^4 muons/sec and proton emission rate of 0.15 per muon capture are assumed. The efficiency of Si detector of 100 % is also assumed.

Target thickness (μm)	Muon momentum (MeV/c)	% Stopping in target	Event rate (Hz) All particles	Event rate (Hz) Protons
50	26	22.2	34.8	4.6
100	27	32.9	48.5	5.4
150	28	38.5	54.5	4.8
200	28	51.2	47.7	4.5

4.2 Gamma and X-ray emission after Muon Capture

The conversion experiment proposes to monitor the number of stopped muons by measuring the various muonic X-rays generated by the captured muons as they cascade down to the muonic atom ground state. We propose to test this scheme at PSI, as well as two alternate normalization methods.

At PSI, we propose to install a high-purity germanium detector at a port in the stopping target vacuum vessel to measure the rate of muonic X-ray production and hence the number of muons stopped in the target. Table 6 lists the most prevalent gamma rays from the Si, Al, and Ti targets. Typical energy resolution of the HPGe detector will be of order 2 keV for 1 MeV photons. Normalization of the other measurements in this proposal will rely on the HPGe detector, although use of an active Si target will provide a useful cross-check.

A mechanical cooling system will be provided for the HPGe detector, eliminating the need for a liquid nitrogen supply, although cooling with cryogens is still a possibility if the mechanical system is deemed insufficient. A high-speed, 14-16 bit data acquisition system will be used to record and store high-resolution raw waveforms for offline analysis, although real-time spectra will also be available for monitoring. The raw data stream will be provided to the DAQ systems of the other detectors.

Measurements of particular interest using the Mu2e germanium detector include the muonic X-ray and gamma spectra as well as careful analysis of both immediate and long-term effects of neutron on the detector. Fast neutrons can create spurious peaks due to excitation of Ge nuclei through inelastic neutron scattering, background signals from activation products in both the detector and surrounding cryostat, and long-term resolution degradation due to creation of hole-trapping defects in the germanium lattice. The distance between the target and HPGe detector in the PSI experiment will be selected such that long-term damage to the HPGe is minimized, although the actual neutron

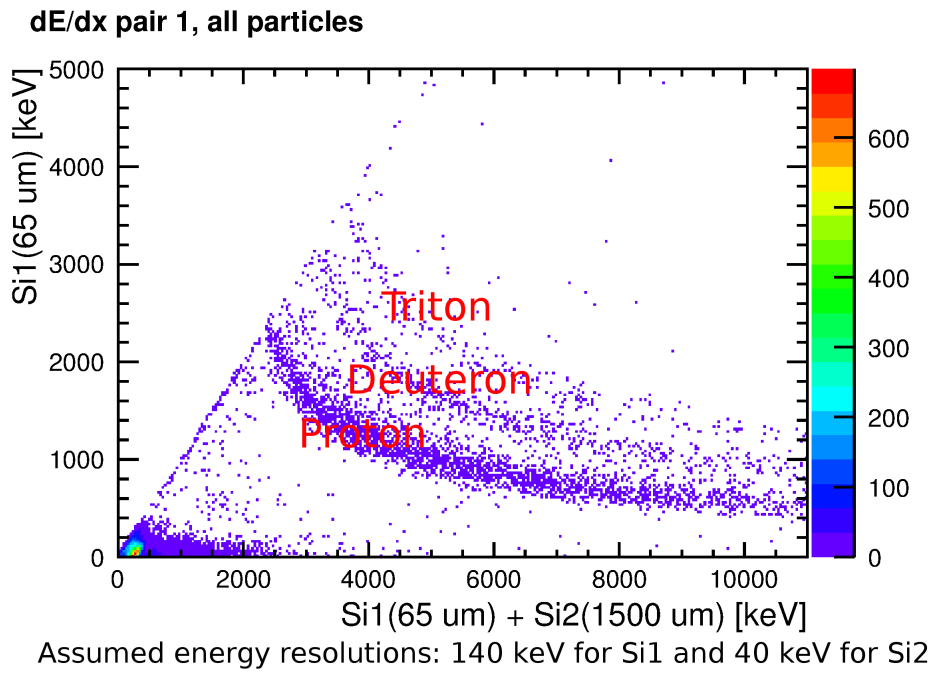

Figure 14: Two dimensional plots of energy deposit in Si1 (65 μm) vs sum of that in Si1 (65 μm) and Si2 (1500μm) (horizontal) counters. The protons can be distinguished from deuterons and tritons in the range of 2.5 − 10 MeV. The low energy particles near zero point are electrons and photons.

flux is expected to be small.

A large NaI detector will be used to measure the high energy photons from the muon stopping target, with the primary goal of evaluating alternative means of monitoring the stopped muon rate. Photons from radiative muon decay have a probability distribution that decreases to nearly zero at about 54 MeV. The NaI detector has 9 PMTs viewing a large single crystal, whose signals will be digitized using waveform digitizers and then fed into the regular DAQ data stream. The rate of photons from radiative muon capture, ranging up to about 80-90 MeV, will also be measured.

Table 6: Energies of muonic X-rays in selected target elements.

Transition	Si (keV)	Al (keV)	Ti (keV)
$2p \rightarrow 1s$	400	347	1021
$3p \rightarrow 1s$	477	413	1210
$4p \rightarrow 1s$	504	436	1277
$3d \rightarrow 2p$	77	66	189

4.3 Neutrons Emission after Muon Capture

The measurement of neutron emission after muon capture proposes to use an Al target of sufficient width and depth to capture and stop all muons from the low momentum beam incident on the target. The emitted neutrons are to be detected with counters using pulse shape discrimination, as described below, with detector readout is triggered by muon entry into the target. The number of captured muons is given by counting the muonium x-rays, as described previously. A beam rate of a few kHz prevents signal overlap in the detector(s) and provides a sufficient statistical sample in a few days.

4.4 Simulation

A particle emission simulation was obtained using the FLUKA simulation code, version FLUKA2011.2.. The model uses a thick, cylindrical target of pure Al. The incident low energy muon is completely stopped in the target, and is captured in an atomic orbit. The captured muons are then allowed to decay in orbit (DIO) or capture in the Al nucleus with nucleon emission, as well as photons and a muon neutrino. The simulation of the energies of the neutron, proton, and gamma particles emitted after μ capture in Al is shown in Figure 15. Emission from a Si target is similar. The Si target does have approximately 25% more gamma emission, with the excess gammas at very low energies. The simulation produces a ratio, 0.57, of gammas above 0.5 Mev per μ capture, and a ratio, 0.72, of gammas per emitted neutron. The correlation between neutron and gamma emission is shown in a correlation plot of neutron vs gamma energy in Figure 16. In this plot the highest neutron energy is plotted against the highest gamma energy, so multiplicities are not counted. The simulated spectrum only includes prompt photons.

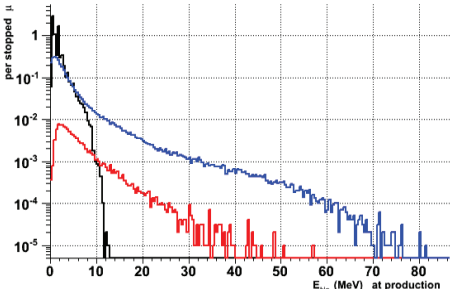

Figure 15: The FLUKA simulated spectrum for proton(red), neutron(blue), and gamma(black) emission per μ stop after μ capture on Al

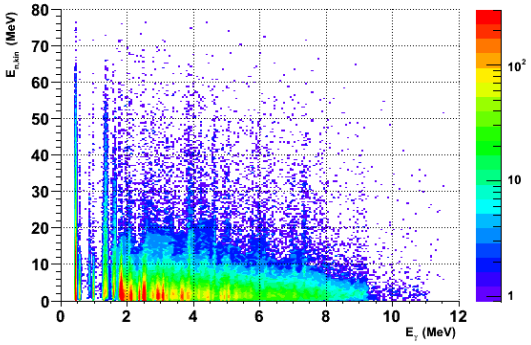

Figure 16: A FLUKA simulation of the energy correlation between neutron (vertical) and prompt gamma (horizontal) emission after μ capture on Al

4.5 Determination of the Neutron Spectrum

While we are still evaluating the possibility of the neutron TOF measurement to determine the neutron energy distribution, we propose the use of neutron spectrum unfolding techniques [20]. The information used in this method requires the measured pulse energy for each detector hit and a detector response function, $R(E, E')$. For a neutron energy spectrum $\phi(E)$, the measured detector response $N(E')$ is given by:

$$N(E') = \int_E R(E, E') \cdot \phi(E)\, \mathrm{d}E, \tag{4}$$

If $R(E, E')$ is well known, the neutron energy spectrum can be obtained by unfolding the measured energy distribution with $R(E, E')$. In this method, the TOF is not used but only the pulse integral to obtain $N(E')$ of the neutrons coming from the target. Therefore, the detector can be moved closer to the muon stopping target when compared to the TOF method.

Response function, $R(E, E')$, measurements with known neutron energy distributions spanning the entire energy range of interest, have to be obtained. This can be achieved with a combination of different neutron sources, specific reactions with emission of mono-energetic neutrons, or measurements at facilities with neutrons of known energy distribution. We will explore the optimal choice such input measurements over the next weeks in order to calibrate $R(E, E')$ prior to mounting the experiment at PSI. We have had initial discussions with the TUNL facility on this matter. While it would be advantageous to measure $R(E, E')$ ahead of running the experiment, we could still proceed with the

measurements at PSI if $R(E, E')$ was not fully quantified.

Over the course of the next weeks, we intend to test existing unfolding codes [20] with Monte Carlo generated input test distributions $\phi(E)$ and typical detector response functions $R(E, E')$. We also intend to study the influence of the knowledge of $R(E, E')$ on the precision with which the neutron energy spectrum can be extracted.

4.5.1 Neutron detectors and readout

We propose to use at least one of the six identical neutron counters from the MuSun experiment[2]. These counters are cylindrical cells of 13 cm diameter by 13 cm depth and contain approximately 1.2 liters of BC501A organic scintillator. The cell is coupled to a 13 cm diameter photo-multiplier tube. For comparison, we might also employ one of the two home made neutron detectors which were built by Regis University. While they are similar in size to the six BC501A ones, these detectors are filled with the EJ-301 and EJ-309 liquid scintillator, respectively. However, there are no major differences in the three types of available detectors.

Any of these detectors would use 12-bit, 170 MHz custom-built waveform digitizers, and an eight channel board from the MuSun experiment is available. Each board can sustain data rates of a few MB/s before loss of data packages occurs. While the expected neutron rates are well below this limit, additional background rates in the experimental hall can be suppressed by sufficient shielding around the detector. Fig. 17(a) shows a typical, digitized signal from one of the BC501A neutron detectors with 5.88 ns binning (170 MHz). The full digitization of each signal allows separation of neutrons from gammas by means of pulse shape discrimination (PSD). The two dimensional plot in Fig. 17(b) of the so-called slow integral (the sum of the bins 5 to 20 to the right of the signal peak in Fig. 17(a)) versus the total integral reveals two distinct bands. The lower band are γ's mainly from the background in experimental hall whereas the upper band is composed of the neutrons. Both integrals are expressed in terms of the electron-equivalent energy which were obtained from calibrations with ^{60}Co and ^{137}Cs sources.

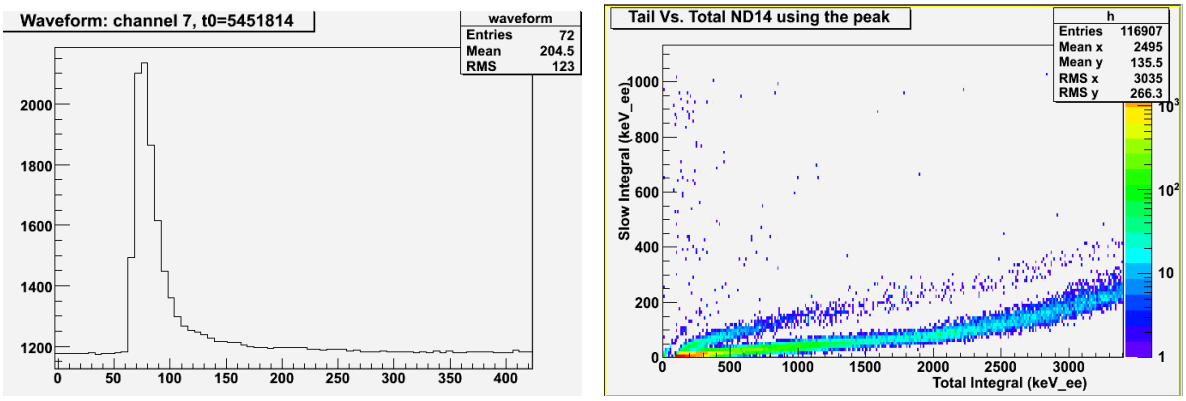

(a) (b)

Figure 17: a) Digitized signal from a BC501A neutron detector (x-axis in ns). b) Neutron-gamma separation via pulse shape discrimination. The slow integral corresponds to the sum of the bins 5 to 20 to the right of the peak of the digitized signal. The lower band contains γs and the upper band the neutrons.

The PSD analysis of the fully digitized neutron signals has been successfully employed in the MuSun experiment. The distance between the neutron and the γ peaks divided by the sum of their FWHM defines the figure of merit M. A higher value of M indicates a better performance. It should be mentioned that the waveform digitizer board was optimized for these neutron detectors by fine tuning a low-pass filter on the analog input. This led to a significant improvement of the figure of merit M.

[2] http://muon.npl.washington.edu/exp/MuSun/

Currently $M = 1$ is achieved at an electron-equivalent energy of 200 keV corresponding to a neutron energy of about 0.7 MeV (MuSun analysis, see also [21]).

5 Organization

5.1 Organization and Responsibilites

The organization and responsibilities for the three work packages is given below.

Table 7: Main responsibilities for work packages of the AlCap experiment

Work Package	Set-up	Detectors	Electronics	DAQ	Simulation/Analysis
WP1	UW, OU	UW, OU, FNAL	UW, OU	OU, UCL	OU, UCL, UW
WP2	PNNL	PNNL, BU	PNNL,UW	PNNL, OU	PNNL, BU
WP3	UH, ANL	UH, UW	ANL	ANL, OU	UH, ANL

5.1.1 WP1

We have a vacuum chamber and Si detectors, which were used for a similar measurement at PSI in 2009. The vacuum chamber is being tested now at University of Washington (UW). The two exiting Si detectors are also being tested at UW. A possibility to prepare another set of Si detectors is being considered. Amplifiers for the existing SI detects are available. The Osaka University (OU) group is preparing DAQ system based on a PSI standard data acquisition system (MIDAS). Monte Carlo simulations necessary to optimize detector configuration is undergoing at OU and University College London (UCL).

Data will be analyzed independently at Osaka University, University of Washington, and University College London, using standard analysis libraries and our own analysis routines. There is no special requirement on data analysis support to PSI.

5.1.2 WP2

PNNL has a number of HPGe detectors available; one appropriate for the experiment will be chosen and tested in advance. A mechanical cooling system is currently under test at PNNL as well and is expected to be used at PSI. Due to the desired high rate and resolution requirements for the raw HPGe pulse data, PNNL will provide its own DAQ system for data collection. The raw data will be provided to the other DAQ system if desired, and the coordination and timestamps between the two systems will be handled carefully.

HPGe data will be analyzed at Pacific Northwest National Laboratory using standard analysis libraries and our own analysis routines. There is no special requirement on data analysis support to PSI.

5.1.3 WP3

As mentioned above, we plan to use existing neutron detectors and readout electronics provided by the MuSun collaboration. We are also considering to build a small neutron detectors, with optimal resolution. We plan to calibrate the detectors before the final experiment and have started to study and test unfolding methods.

5.2 Requests to PSI

We request limited hardware support from PSI. This includes

1. A temperature controlled tent for the set-up - probably the MuSun installation can be used,

2. 4 NIM and 1 VME crate and 2 racks,

3. Standard NIM electronic modules, to be specified.

4. Availability of liquid nitrogen for cooling of the germanium detector, if the mechanical cooler is identified as insufficient.

References

[1] Y. Kuno and Y. Okada, "Muon decay and physics beyond the standard model," *Rev.Mod.Phys.*, vol. 73, pp. 151–202, 2001.

[2] A. deGouvea, "(Charged) Lepton Flavor Violation," *Nucl. Phys. B (Proc. Suppl.)*, vol. 188, pp. 303–308, 2009.

[3] W. Bertl *et al.*, "A Search for μ-e conversion in muonic gold," *Eur. Phys. J., C*, vol. 47, pp. 337–346, 2006.

[4] R. M. Carey *et al.* (Mu2e Collaboration), "Proposal to search for $\mu^- N \to e^- N$ with a single event sensitivity below 10^{-16}," 2008.

[5] Y. Cui *et al.* (COMET Collaboration), "Conceptual design report for experimental search for lepton flavor violating mu- - e- conversion at sensitivity of 10^{-16} with a slow-extracted bunched proton beam (COMET)," 2009.

[6] S. Sobottka and E. Wills, "Energy Spectrum of Charged Particles Emitted Following Muon Capture in Si^{28}," *Phys. Rev. Lett.*, vol. 20, pp. 596–598, 1968.

[7] E. Hungerford, "Comment on Proton Emission after Muon Capture, MECO Note 34."

[8] M. Lifshitz and P. Singer, "Nuclear excitation function and particle emission from complex nuclei following muon capture," *Phys. Rev. C*, vol. 22, pp. 2135–2150, 1980.

[9] K. S. Krane, T. C. Sharma, L. W. Swenson, D. K. McDaniels, P. Varghese, B. E. Wood, R. R. Silbar, H. D. Wohlfahrt, and C. A. Goulding, "Energetic charged-particle spectrum following μ^- capture by nuclei," *Phys. Rev. C*, vol. 20, pp. 1873–1877, 1979.

[10] V. Balashov and R. Eramzhyan, *Atomic Energy Reviews 5*, 1967.

[11] D. Measday *et al.*, "Gamma rays from muon capture in Al-27 and natural Si," *Phys. Rev. C*, vol. 79, 2007.

[12] A. Czarnecki, et al, *Phys. Rev. D*, vol. 85, p. 025018, 2012.

[13] E. B. Shera, "Pionic and muonic atoms," *Nucl. Phys. A*, vol. 335, pp. 75–82, 1980.

[14] F. Cannarta, R. Graves and H. Uberall, "The Capture of Muons by Complex Nuclei," *Riv. Nuovo Cim.*, vol. 7, 1977.

[15] M. Plett *et al.*, "Effects of the giant resonance on the energy spectra of neutrons emitted following muon capture in C-12 and O-16," *Phys. Rev. C*, vol. 3, pp. 1003–1010, 1971.

[16] B. MacDonald *et al.*, "Neutrons from Negative-Muon Capture," *Phys. Rev. B*, vol. 139, pp. 1253–1263, 1965.

[17] A. Wyttenbach *et al.*, "Probabilities of Muon Induced Nuclear Reactions Involving Charged Particle Emission," *Nucl. Phys. A*, vol. 294, pp. 278–292, 1978.

[18] R. Sundelin *et al.*, "Neutron asymmetries and energy spectra from muon capture in Si, S, and Ca," *Phys. Rev. C*, vol. 7, pp. 1037–1060, 1973.

[19] P. Kammel, Y. Kuno *et al.* (AlCap collaboration), "TRIUMF Experiment S1371: Study of Muon Capture for Muon to Electron Conversion Experiments," 2012.

[20] S. G. R. Koohi-Fayegh and M. Scott, "A comparison of neutron spectrum unfolding codes used with a miniature NE213 detector," *Nuclear Instrumqents & Methods A*, vol. 460, pp. 391 – 400, 2001.

[21] N. Nakao *et al.*, "Measurements of response function of organic liquid scintillator for neutron energy range up to 135 MeV," *Nuclear Instruments & Methods A*, vol. 362, pp. 454 – 465, 1995.